Energy-gap modulations of graphene ribbons under external fields: A theoretical study

C. Ritter,[1] S. S. Makler,[1,2] and A. Latgé[1]
[1]*Instituto de Física, Universidade Federal Fluminense, 24210-340 Niterói-RJ, Brazil*
[2]*Departamento de Física—ICE, Universidade Federal de Juiz de Fora, Juiz de Fora-MG, Brazil*
(Received 22 February 2008; revised manuscript received 29 April 2008; published 29 May 2008)

Here, we address a theoretical study of electronic properties of carbon ribbons under the effect of external electric and magnetic fields. The Peierls approximation is used to incorporate the magnetic field within a tight-binding picture. A charge self-consistent calculation is adopted to analyze the gap modulations induced by the application of the external electric field and compared with simple models. We show that depending on the ribbon geometries and field intensities, a large variety of electronic situations may be achieved, suggesting possible mechanisms for gap engineering of such carbon nanomaterials.

DOI: 10.1103/PhysRevB.77.195443 PACS number(s): 73.21.−b, 73.22.−f, 81.07.−b

I. INTRODUCTION

Ribbon shaped graphene systems do not merely serve as a playground to theoretical physicists who may certainly play with their interesting electronic and transport properties. Actually, they have become an experimental realization after the discovery of single-layer graphene.[1] An example is the *e*-beam lithography technique used in graphene layers to create such narrow graphene nanoribbons.[2] Transport measurements on lithographically patterned graphene ribbon structures have demonstrated the ability to engineer their energy band gaps.[3] By choosing appropriate ribbon widths, it is possible to tune a desired energy gap. The zigzag graphene nanoribbon (ZGNR) has intriguing peculiarities; the most important being the exhibition of edge states manifested as prominent peaks in the density of states at the Fermi energy. They come from localized states at both ribbon boundaries and have important consequences on the magnetic properties of these nanostructures. Interesting discussions concerning their potential use as spintronic systems have been addressed recently in the literature as well as the predictions of being good candidates for exhibiting half-metallic properties.[4] Contrarily to that, other authors have suggested a half-semiconductor behavior.[5] Transport properties in graphene strips have been recently reported,[6] showing that a magnetic field provides interesting effects on the typical conductance plateaux.

Motivated by the variety of changes that may be induced in graphenelike nanostructures, similarly to the case of carbon nanotubes, we investigate here the energy-gap modulations induced by external fields. Magnetic fields have been largely used in different systems as a possible way of tuning different length scales and controlling different confinement effects.[7–9] Electronic gap modulations are discussed here, considering the effects of a magnetic field applied perpendicularly to the graphene ribbon structure. Actually, new effects in graphene in the presence of crossed uniform electric and magnetic fields are reported in a quite recent work.[10] More precisely, they predicted a collapse of the entire Landau level structure. Graphene strips under transversal electric fields are also studied within a self-consistent model calculation. How the energy gap depends on the field intensity and on the ribbon geometry is analyzed. It was previously shown that a transverse voltage applied across nanoribbon systems may dramatically change the corresponding electronic energy dispersion.[11] Both self-consistent (SC) and simple noniterative calculations show a threshold for the electric field that lead to gap modulations and metallic transitions. One has found a higher threshold when adopting the SC calculation, as expected.

II. THEORY AND RESULTS

Here, we restricted our study to zigzag N_z-ZGNR and armchair N_a-AGNR, nanoribbon families. They are standard strips of graphitelike nature presenting zigzag and armchair shaped edges on both sides, and composed of transversal atomic chains having $2N_z$ and N_a carbon atoms, respectively. A schematic view of such ribbons is displayed in Fig. 1, with the corresponding unit cells and first-neighbor vectors given by $\mathbf{R}_n$. The graphene ribbons are described by a single-band tight-binding Hamiltonian written in the real space and given by

$$H = \sum_{n}^{N} \epsilon_n(E) c_n^{\dagger} c_n + \sum_{n,m}^{N} \gamma_{n,m}(B) c_n^{\dagger} c_m + h\,.\,c.\,, \qquad (1)$$

with $\epsilon_n(E)$ being the electrical-field–dependent site energy, and $\gamma_{n,m}(B)$ the energy hopping between first-neighbor atoms, which incorporates the magnetic field B. For $B=0$, one has $\gamma_{n,m}=\gamma_o \approx 2.7$ eV. The effect of passivating the carbon atoms displayed at the ribbon edges with hydrogen is better described when considering hybridizated σ orbitals.[12] How-

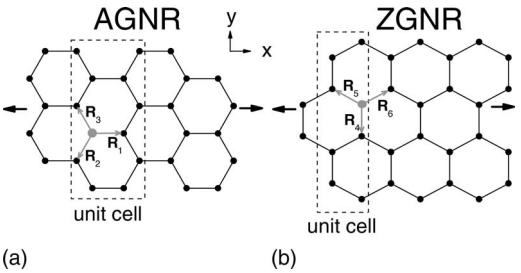

FIG. 1. Schematic view of a typical (a) AGNR and (b) ZNGR, with the respective unit cells and first-neighbor vectors.

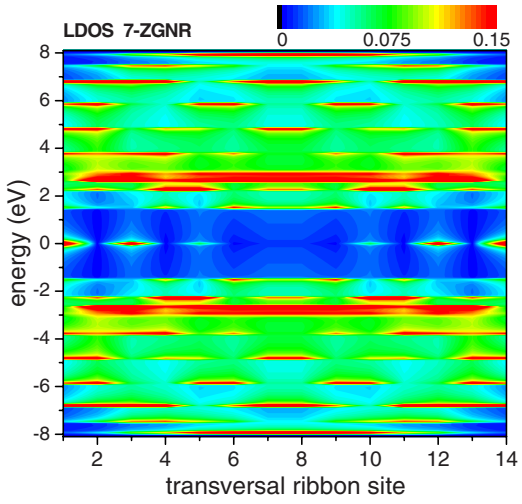

FIG. 2. (Color online) LDOS map for a 7-ZGNR. Results for the local density of state as a function of energy, for each one of the carbon sites displayed along the transversal direction are plotted. The up label indicates the LDOS intensity.

ever, for single π orbital model, a position-dependent hopping amplitude may be adopted to model the effect of hydrogen passivation. For armchair ribbons, the hopping energy between the carbon atoms layering in the dimmer position of the external boundary strip is modeled by $\gamma=\gamma_o(1+\delta)$, following a previous analysis performed on the basis of *ab initio* calculation,[13] which predicts an increasing hopping of the order of 12% (i.e., $\delta=0.12$).

Local densities of states (LDOS) are calculated by using the Green function formalism. Renormalized locators are calculated from a Dyson equation scheme to get local densities of states at the ribbon sites. Results for the LDOS are shown in Fig. 2 for a particular ZGNR configuration. The edge states near the Fermi energy exhibit peaks at the LDOS which are marked in the diagram map. A robust signature of the quasi-one-dimensional lattice is found at the energy corresponding to $\pm\gamma_o$, by the well defined van Hove singularity exhibited for almost all the local density of states corresponding to the different sites.

A. Magnetic-field effects

Following the same model calculation adopted previously on carbon nanotubes,[14–16] we use the Peierls approximation to describe the effects of a magnetic field applied perpendicular to the carbon ribbon plane. In that sense $\gamma_{n,m} \rightarrow \gamma_{n,m}e^{2\pi i\Delta\Phi_{n,m}}$, with the phase $\Delta\Phi_{n,m}$ given by the line integral of the vector potential $\mathbf{A}$,

$$\Delta\Phi_{n,m} = e/h\int_{\mathbf{R}_n}^{\mathbf{R}_m} d\mathbf{l}\,.\,\mathbf{A}. \tag{2}$$

The resulting phase factors found for the armchair ribbon configuration are given by the following expressions:

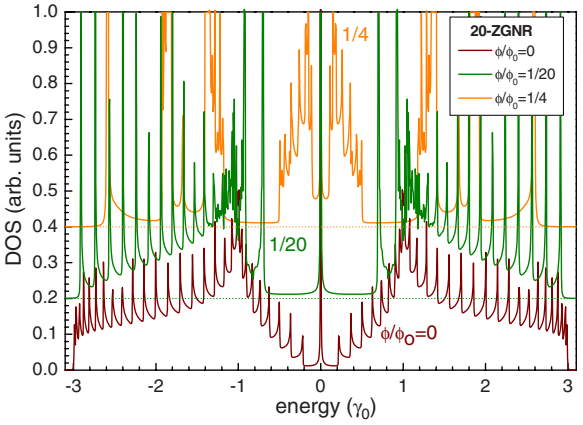

FIG. 3. (Color online) Total DOS of a 20-ZGNR for different magnetic fields. The curves are shifted upward to help the visualization.

$$\Delta\Phi_{n,m} = \begin{cases} \pm aBx_n & \text{if } \mathbf{R}_{n,m} = \pm\mathbf{R}_1 \\ \dfrac{aB}{2}\left[\pm x_n - \dfrac{a\sqrt{3}}{4}\right] & \text{if } \mathbf{R}_{n,m} = \mp\mathbf{R}_2 \\ \dfrac{aB}{2}\left[\pm x_n + \dfrac{a\sqrt{3}}{4}\right] & \text{if } \mathbf{R}_{n,m} = \mp\mathbf{R}_3 \end{cases} \tag{3}$$

with $\mathbf{R}_1=a\hat{\mathbf{y}}$, $\mathbf{R}_2=-(\sqrt{3}\hat{\mathbf{x}}+\hat{\mathbf{y}})a/2$, $\mathbf{R}_3=(\sqrt{3}\hat{\mathbf{x}}-\hat{\mathbf{y}})a/2$, $a=|\mathbf{R}_{n,m}|$, and $n\leq 2N$. For the zigzag ribbons, one gets

$$\Delta\Phi_{n,m} = \begin{cases} 0 & \text{if } \mathbf{R}_{n,m} = \pm\mathbf{R}_4 \\ \dfrac{\sqrt{3}aB}{2}\left[\pm x_n + \dfrac{a}{4}\right] & \text{if } \mathbf{R}_{n,m} = \pm\mathbf{R}_5 \\ \dfrac{\sqrt{3}aB}{2}\left[\pm x_n - \dfrac{a}{4}\right] & \text{if } \mathbf{R}_{n,m} = \pm\mathbf{R}_6 \end{cases}, \tag{4}$$

with $\mathbf{R}_4=-a\hat{\mathbf{x}}$, $\mathbf{R}_5=(\hat{\mathbf{x}}-\sqrt{3}\hat{\mathbf{y}})a/2$, $\mathbf{R}_6=(\hat{\mathbf{x}}+\sqrt{3}\hat{\mathbf{y}})a/2$.

The magnetic fluxes are written in terms of the flux threading a single lattice hexagon ($3\sqrt{3}a^2B/2$) expressed in units of the quantum flux $\phi_o=h/e$ (for $\phi/\phi_o=10^{-3}$ one has $B=79$ T). The dependence of the DOS on the magnetic field

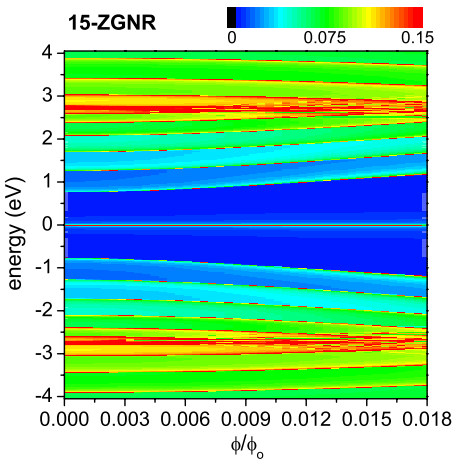

FIG. 4. (Color online) Diagram DOS map as a function of the magnetic flux threading a hexagonal ring for a 15-ZGNR.

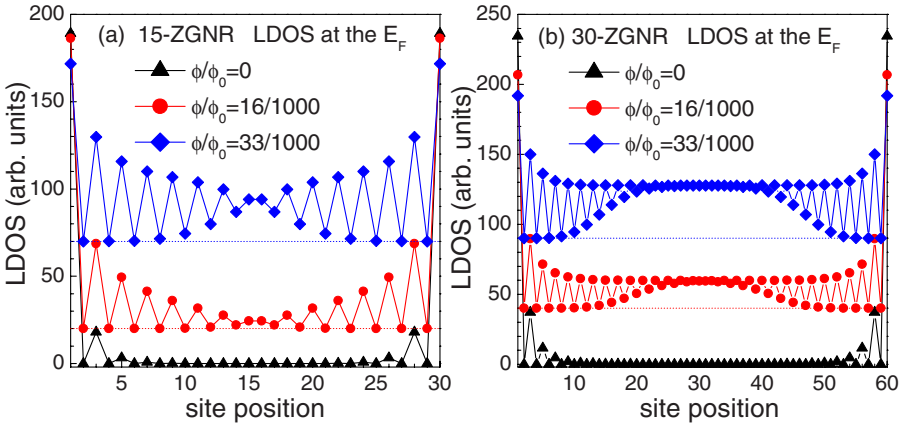

FIG. 5. (Color online) LDOS at the Fermi level (E_F=0) for N_z-ZGNRs, with N_z equal to (a) 15 and (b) 30, at the sites along the ribbon transversal direction. Different values of the magnetic flux are considered.

for a zigzag ribbon is shown in Figs. 3 and 4. One clearly notices a concentration of states at particular energy ranges driven by the field intensity. The evolution of van Hove singularities may also be noticed as the magnetic flux is increased by the marked curves in the DOS diagram map exhibited in Fig. 4. Also, it is interesting to notice the effects of the magnetic flux intensity on the density of states at the Fermi energy for different sites of the ribbon. The extra electronic confinement imposed by the magnetic field and given by the Landau radius, leads to an increasing of zero-energy Landau level. It may clearly be seen, in Fig. 5, the zero-energy edges states evolving into zero-energy Landau levels that spread into the system bulk for different values of magnetic flux. When analyzing the situation for armchair ribbons, under magnetic fluxes, one notes an intriguing picture: depending upon quite small changes in the ribbon size, the gap evolution presents remarkable different behavior for increasing fields, as shown in Fig. 6. Under the action of B, the gap energy increases for a 24-AGNR, decreases for a 25-AGNR, and exhibit mixed features for N_a=26. In the last

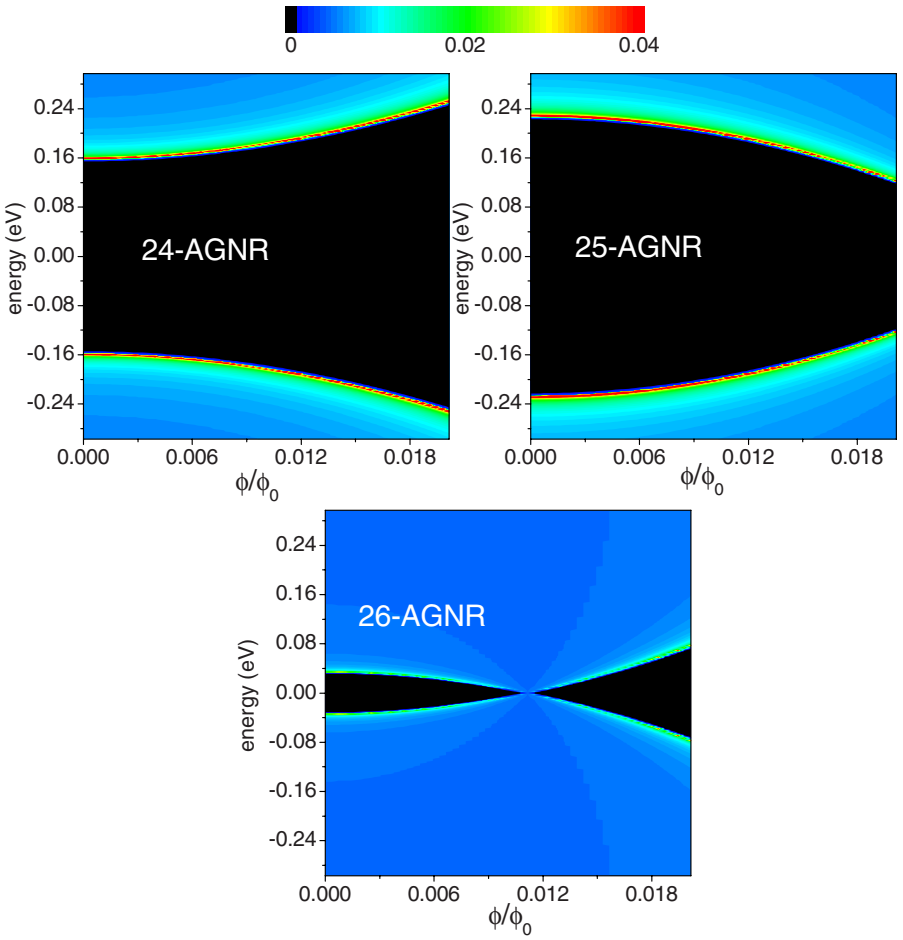

FIG. 6. (Color online) Energy-gap dependence on the magnetic field for N_a=24, 25, and 26 N_a-AGNRs.

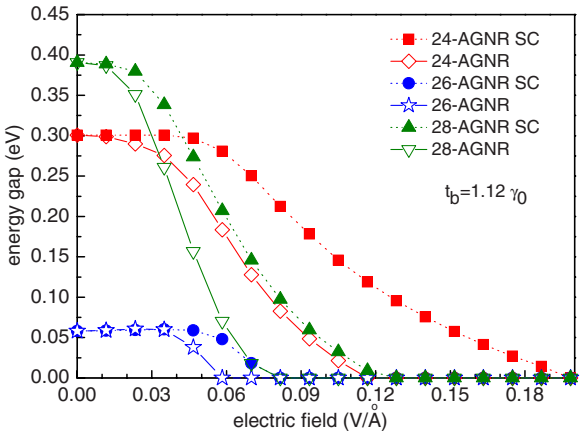

FIG. 7. (Color online) Energy gap of N_a-AGNRs as function of the electric field. Results for the SC calculations are shown in bold symbols for N_a=24, 26, and 28, and compared with nonself-consistent ones (opened symbols).

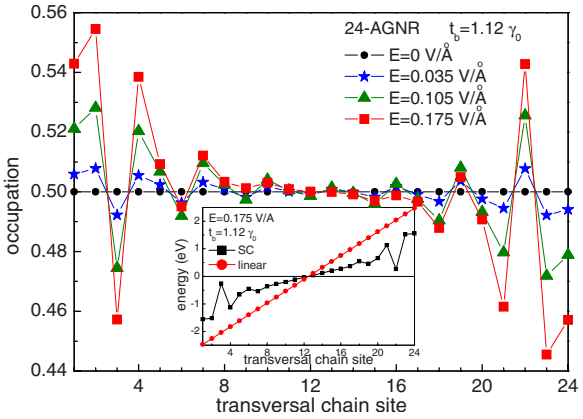

FIG. 8. (Color online) Local charge occupation for a 24-AGNR for different values of the electric field. Inset: linear potential and self-consistent potential for an applied filed equal to 0.0175 V/Å.

case, the graphene ribbon belongs to an armchair family for which, naive tight-binding models do not predict a semiconducting nature.[13]

B. Electric-field effects

Changes on the gap sizes are also predicted when an electric field is applied in the transversal direction of armchair ribbons.[17–19] Usually, a simple scheme is adopted, in which $\epsilon(E)$, the diagonal term of the Hamiltonian [Eq. (1)], varies linearly from $-U/2$ to $U/2$ across the ribbon sites, with the potential energy given by $U=-eEd$, d being the ribbon width. Following this model, we have first analyzed the dependence of the gap size as a function of the electric-field intensity. Different passivation models were taken into account via renormalization of the hopping site energies, corresponding to the C-H bonds at the edges, or by considering dressed carbon atoms at those positions with different site energies. However, as previously predicted, both schemes have provided no substantial changes in the behavior of the gap electric-field dependence, as compared to the results found for the bare ribbon structures. On the other hand, an important point is the inclusion of charge effects mainly due to the low dimensionality of the structure and the edge effects. With this purpose, we consider the hexagonal ribbon systems as being described by a finite set of charge lines and calculate the electrostatic potential at each one of these lines using a continuous approximation. The potential $\Phi(y)$ is then given by a finite superposing of the contribution of all other charge lines, and is given by

$$\Phi(y_m) = -\sum_{n\neq m} \frac{\lambda_n}{2\pi\epsilon} \ln\left|\frac{y_m - y_n}{y_o - y_n}\right|, \qquad (5)$$

with ϵ being the graphene permittivity constant, considered[11] equal to $5\epsilon_o$ and λ_n, the corresponding local charge densities obtained by integration of the local Green function in the complex plane. y_n denotes the continuous charge lines, along the x axis, with n varying from 1 to N in the transversal direction. An arbitrary origin y_o is taken at the center of the system to maintain the symmetry of the problem and define the zero-energy potential.

A self-consistent calculation for the local charges is performed via a quasi-Newton numerical procedure.

Results for the gap evolution as the electric-field intensity increases are shown in Fig. 7 for N_a-AGNRs, with N_a=24, 26, and 28. Self-consistent calculations are compared with

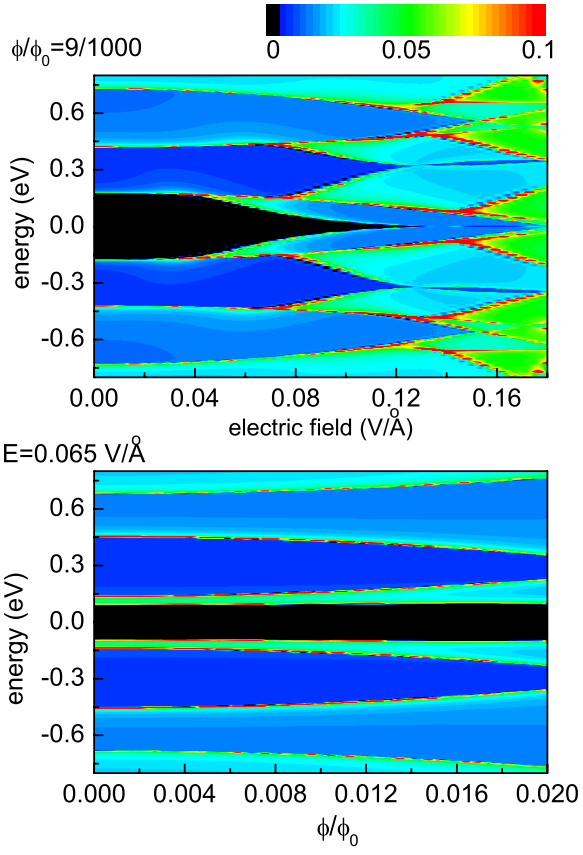

FIG. 9. (Color online) LDOS diagram plot for a 24-AGNR as a function of the electric field for Φ/Φ_o=9/1000 (top panel), and the magnetic flux for E=0.065 V/Å in the bottom panel. Black regions correspond to null density of states while the highest value of LDOS are exhibited in bright lines (yellow color online).

those without including the charging effects. For quite small values of the transverse electric field, both results coincide and the differences start to increase for higher fields but maintaining the general trend. Therefore, the field-induced semiconductor-metallic transition actually takes place for higher fields than the critical value predicted by the simple[17] and not self-consistent model (linear-dependent potential), depending also on the ribbon width. To highlight the effects of the self-consistent procedure on the potential energy, we plot the charge distribution along the transversal direction (y axis) for a 24-AGNR, considering different electric-field values (see Fig. 8). The linear interpolation of the electric-field energy and the self-consistent result using Eq. (5) are displayed at the inset, for $E=0.175$ V/Å, for comparison. When applying an electric field, rearrangement of the charge distribution takes place. The resulting polarized medium acts, reducing the effect of the external field as can be seen in the inset of Fig. 8. Contrarily to armchair nanoribbons, ZGNR systems present a metallic behavior. When an electric field is turned on, the energy gap starts to open and increases with the electric field. At a critical value, which depends on the ribbon width, it again decreases as a function of the field intensity. A self-consistent analysis also leads to a reduction of the electric-field effects, as expected. For the sake of conciseness, these results are not shown here.

C. Both electric and magnetic fields

Results for the density of states of a 24-AGNR as function of the applied fields (electric and magnetic) are finally shown in Fig. 9 using (colored on-line) diagram plots. One interesting result is the enhancement of the energy band changes as the transversal electric field increases when the system is under the action of a perpendicular magnetic field. The gap modulation sensibility is further increased for higher applied magnetic fields. These effects could offer additional possibilities of tuning the energy gaps, which is for sure, an important characteristic of those AGNR nanostructure. Otherwise, as shown in the lower panel, for a fixed electric-field value ($E=0.065$ V/Å) the central gap size is quite robust against changes of the magnetic field. Gap modulations of ZGNRs under the effects of both the fields, have also been investigated, although the results are not shown here. Besides the opening of the energy gap under applied electric fields, extra gap modulations are achieved by the additional magnetic field. Such analysis should be presented elsewhere.

Admittedly, external magnetic fields required to evidence the effects shown in our results are beyond present experimental possibilities. On the other hand, we should emphasize that only quite narrow ribbons were considered in this study and lower magnetic field values provide similar effects for wider ribbons. The reduced size systems are used just to highlight general trends. Despite of the simplicity of the model calculation adopted here, the results unambiguously indicate a number of channels to get desirable changes on the electronic properties of graphene nanoribbon systems.

ACKNOWLEDGMENTS

We acknowledge the financial support of Brazilian agencies, CAPES CNPq, and Instituto do Milênio de Nanotecnologia.

[1] K. S. Novoselov and A. Geim, Nature (London) **438**, 197 (2005).
[2] B. Obradovic, R. Kotlyar, F. Heinz, P. Matagne, T. Rakshirt, M. D. Gilles, M. A. Stettler, and D. E. Nikonov, Appl. Phys. Lett. **88**, 142102 (2006).
[3] M. Y. Han, B. Ozyilmaz, Y. Zhang, and P. Kim, Phys. Rev. Lett. **98**, 206805 (2007).
[4] Y.-W. Son, M. L. Cohen, and S. Louie, Nature (London) **444**, 347 (2006).
[5] E. Rudberg, P. Salek, and Y. Luo, Nano Lett. **7**, 2211 (2007).
[6] N. M. R. Peres, A. H. Castro Neto, and F. Guinea, Phys. Rev. B **73**, 195411 (2006).
[7] Y. C. Huang, C. P. Chang, and M. F. Lin, Nanotechnology **18**, 495401 (2007).
[8] L. Brey and H. A. Fertig, Phys. Rev. B **73**, 235411 (2006); **73**, 195408 (2006).
[9] J. H. Ho, Y. H. Lai, Y. H. Chiu, and M. F. Lin, Nanotechnology **19**, 035712 (2008).
[10] V. Lukose, R. Shankar, and G. Baskaran, Phys. Rev. Lett. **98**, 116802 (2007).
[11] D. S. Novikov, Phys. Rev. Lett. **99**, 056802 (2007).
[12] Y. Miyamoto, K. Nakada, and M. Fujita, Phys. Rev. B **59**, 9858 (1999).
[13] Y. W. Son, M. L. Cohen, and S. G. Louie, Phys. Rev. Lett. **97**, 216803 (2006).
[14] K. Wakabayashi, M. Fujita, H. Ajiki, and M. Sigrist, Phys. Rev. B **59**, 8271 (1999).
[15] C. G. Rocha, A. Latgé, and L. Chico, Phys. Rev. B **72**, 085419 (2005).
[16] A. Latgé and D. Grimm, Carbon **45**, 1905 (2007).
[17] C. P. Chang, Y. C. Huang, C. L. Lu, J. H. Ho, T. S. Li, and M. F. Lin, Carbon **44**, 508 (2006).
[18] R. Saito, G. Dresselhaus, and M. Dresselhaus, J. Appl. Phys. **73**, 494 (1993).
[19] K. H. Ahn, Y. H. Kim, J. Wiersig, and K. J. Chang, Phys. Rev. Lett. **90**, 026601 (2003).